Journal of Chromatography, 562 (1991) 153–168
Biomedical Applications
Elsevier Science Publishers B.V., Amsterdam

CHROMBIO. 5581

Characteristic fragmentation of thromboxane B_2 in thermospray high-performance liquid chromatography–mass spectrometry

J. ABIÁN and E. GELPÍ*

Department of Neurochemistry, CID, CSIC, Jorge Girona Salgado 18-26, 08034 Barcelona (Spain)

ABSTRACT

Cyclo- and lipo-oxygenase metabolites of arachidonic acid have been reported to have very simple thermospray mass spectra. However, thromboxane B_2 (TXB) in ammonium acetate–methanol and at interface temperatures below the point of total vaporization shows a mass spectral pattern characterized by abundant ions at low masses. The more abundant TXB fragment ions have been characterized as adducts from four principal fragments with molecular masses of 156, 170, 196 and 326. Positive- and negative-ion mass spectra, and mass spectra obtained with an alternative thermospray buffer (butylammonium acetate) support the molecular masses of these fragments. A tentative assignment of the fragments can be made by comparison of the thermospray mass spectra of TXB, 2,3-dinor-TXB and some of their methyl ester and methyl oxime derivatives. Interface temperature and solvent composition effects on the fragmentation, as well as in the electron-capture processes observed when working in the filament-on mode, are discussed. Fragmentation mechanisms can be related to those observed for monosaccharides, and imply retro-Diels–Alder as well as retroaldolic condensation-type rearrangements.

INTRODUCTION

Cyclo- and lipo-oxygenase metabolites of polyunsaturated fatty acids play important roles in many physiological processes. Their analysis by thermospray (TSP) high-performance liquid chromatography (HPLC)–mass spectrometry (MS) has been approached by various authors [1–5], and different derivatives such as methyl esters, methoximes and pentafluorobutyl (PFB) oximes have been tested in order to enhance detection limits and/or functional information.

In general, prostaglandins, hydroxyeicosatetraenoic acids (HETEs) and other lineal polyoxygenated fatty acids, such as leukotriene B_4 (LTB_4) and other di-HETEs derived from arachidonic acid, show very simple spectral patterns in TSP–HPLC–MS, mostly due to adduct ions [5], that can be explained following the practical rule recently proposed by Maeder [6]:

$$\text{Ion} = \text{M} + \text{A} + x\text{B} - y\text{C} \quad (1)$$

According to this equation, the m/z of the ions concentrated in the quasimolec-

0378-4347/91/$03.50

ular ion zone can be explained as the sum of the molecular mass value of the analyte (M) plus the m/z values of the ions arising from the eluent in the liquid or gas phase (A). In the addition, ions M + A can also attach eluent molecules (B) or lose neutrals (C). In the case of arachidonic acid metabolites, and with the eluents commonly used for their analysis (ammonium acetate and formate with methanol or acetonitrile (ACN) as organic modifiers), A would be H^+ or NH_4^+, B would be methanol or ACN molecules and C one or more water molecules from dehydration processes. In the negative-ion mode, A would be either acetate or formate ions or a proton loss.

Thromboxane B_2 (TXB) is the most important cyclo-oxygenase metabolite of arachidonic acid in platelets, and is also released from other cells, such as macrophages and polymorphonuclear leukocytes. However, in contrast with other prostanoids, the mass spectral pattern of TXB shows some ions in the quasimolecular ion zone that cannot be explained by simple water losses from the adduct ions. Further, TXB shows high-intensity signals at masses below 250 a.m.u. that cannot be explained by assuming either extensive dehydration or doubly charged species.

The molecular structure of TXB (Fig. 1) is characterized by its pyran ring with a hemiketal structure: this differs from the prostaglandin family, where cyclization affords a cyclopentane ring structure. Some aspects of the MS behaviour of TXB should thus be compared with those of a monosaccharide rather than with those of the other cyclo-oxygenase metabolites.

In this work, positive- and negative-ion mass spectra for TXB and 2,3-dinor-TXB, as well as their methyl esters and methoximes, were recorded under both pure TSP and assisted TSP conditions (with an electron-emitter filament). Different TSP parameters, such as buffer type and interface and source temperatures, were tested. Tentative structures for the observed ions are proposed.

EXPERIMENTAL

Standards and reagents

TXB and 2,3-dinor-thromboxane B_2 (DTXB) were obtained form Upjohn (Kalamazoo, MI, U.S.A.). 1-Methyl-3-nitro-1-nitrosoguanidine (diazomethane reagent) and methoxyamine hydrochloride were obtained from EGA Chemie

Fig. 1. Equilibrium forms of TXB and DTXB. R1 = $(CH_2)_3COOH$ (TXB), R1 = CH_2COOH (DTXB), R2 = $(CH_2)_4CH_3$.

(Steinheim/Albuch, F.R.G.) and Pierce (Rockford, IL, U.S.A.), respectively.

Water used in the HPLC eluents was of Milli-Q grade (Waters Assoc., Milford, MA, U.S.A.) and was passed through a 0.45-μm filter. The other solvents and reagents were of analytical or chromatographic grade.

Chemical derivatives

Chemical derivatives of TXB and DTXB were obtained by well-known procedures (diazomethane for methyl esters and methoxyamine hydrochloride in pyridine for methyloximes) [5]. No purification of the derivatives was performed prior to chromatography.

TSP buffers

A 0.1 *M* ammonium acetate buffer (AMAC) and a 0.1 *M* butylammonium acetate buffer (BUTAC) were used for TSP. The pH was adjusted to 4 with formic acid. Buffers were prepared from ammonium hydroxide or butylamine and acetic acid. In our experience this method affords more pure buffer solutions than from commercial salts.

Mass spectrometry

A Hewlett-Packard 5988A quadrupole gas chromatograph–mass spectrometer with a source for TSP and a Vestal-type interface was used. The source temperature was kept at 250°C. In some cases spectra were also recorded at 200°C and 300°C. In the filament-on mode, the electron energy was set at 250 V.

Calibration

A poly(propylene glycol) mixture (PPG; average molecular mass 425 and 725) in 50% AMAC–ACN at 1 ml/min was used for mass spectrometric calibration. Mass axis calibration was performed employing ions at m/z 141 ($[NH_4 + 3ACN]^+$ from the buffer plasma), 268 and 326 ($[M + NH_4]^+$ from $n = 4$ and $n = 5$ PPG oligomers) for positive ions, and 137, 179 ($[2AcOH + H_2O - H]^-$ and $[3AcOH - H]^-$ adducts from the buffer plasma) and 367 ($[M + AcO]^-$ from the $n = 5$ PPG oligomer) for negative ions (where Ac = acetyl).

HPLC–MS parameters

All spectra recorded were from compounds chromatographed on 5 μm (15 × 0.4 cm I.D.) or 3 μm (6 × 0.46 cm I.D.) Spherisorb ODS-2 reversed-phase columns. Eluents were AMAC or BUTAC buffers with ACN or methanol as organic modifier. ACN and methanol were used in various proportions (30–50%), depending on the type of derivative chromatographed. The flow-rate was 1 ml/min.

The TSP interface probe (STEM) temperature was normally adjusted at 110°C. Temperature effects were also studied in some runs in the range 92–124°C for STEM temperature, which resulted in a range of interface exit (TIP) temperatures between 160 and 250°C with methanol in the mobile phase.

Spectra are the average of several scans, and the plasma background was substracted.

RESULTS AND DISCUSSION

Positive ions

Mass spectral patterns in the positive mode for TXB and its homologue DTXB (Fig. 1) are shown in Table I. DTXB, a biological metabolite of TXB, has a molecular mass 28 mass units lower than its precursor owing to enzymic removal of a C_2H_4 group from the carboxylic lateral chain. Thus, each of the *m/z* values in the table is shifted by 28 mass units relative to one another in order to identify homologous signals for the two compounds.

Ion numbers depicted in Table I are used to correlate these homologous adduct ions with the equivalent signals obtained in other buffers or from different

TABLE I

TXB AND DTXB RELATIVE ION ABUNDANCES AT TWO DIFFERENT ION-SOURCE TEMPERATURES

TSP mode, filament on; positive-ion detection. Eluent, 50% AMAC (0.1 *M*)–MeOH at 1 ml/min.

[Assignment]$^+$	Ion No.	*m/z*		200°C		300°C	
		TXB	DTXB	TXB	DTXB	TXB	DTXB
X + NH_4 − H_2O	3	170	142	–	3	0.6	0.7
X + H	4	171	143	2.5	2.5	4	4
T + NH_4	5	174	X[a]	2.6	–	2.3	–
X + NH_4	6	188	160	100	94	100	100
Y + NH_4 − H_2O	8	196	168	0.6	1.3	1	2.7
Y + H	9	197	169	2.5	3.7	4.8	3.7
T + NH_4	10	X[a]	174	–	4.7	0.7	4.6
Y + NH_4	12	214	186	52	100	33	49
Z + NH_4	13	216	188	5.9	15	6.3	9.2
X + NH_4 + CH_3OH	14	220	192	2.0	4.7	–	–
Y + NH_4 + CH_3OH	17	246	218	–	2.3	–	–
U + NH_4 − 30	27	314	286	0.2	0.5	0.2	0.3
M + H − $3H_2O$	28	317	289	–	0.2	0.8	0.8
U + NH_4 − H_2O	29	326	298	–	1.0	–	0.3
M + NH_4 − $3H_2O$	30	334	306	0.7	1.0	0.3	0.3
M + H − $2H_2O$	31	335	307	0.2	0.3	0.7	0.9
U + NH_4	33	344	316	–	5.0	–	0.4
M + NH_4 − $2H_2O$	34	352	324	0.2	0.5	0.4	0.6
M + H − H_2O	35	353	325	–	0.3	0.4	0.7
M + NH_4 − H_2O	36	370	342	0.4	0.9	1	2.7
M + NH_4	38	388	360	0.7	1.0	0.3	0.4

[a] The corresponding *m/z* ions should not be expected.

TABLE II

PLASMA REAGENT ION RELATIVE ABUNDANCES WITH DIFFERENT HPLC BUFFERS

TSP mode, filament on; positive-ion detection; ion source, 250°C; TSP interface, 100°C, TIP temperature, 100°C. Eluent: 50% B (0.1 *M*, pH 4 with AcOH)–R.

$[Ion]^+$	B = $BuNH_2$		B = NH_3	
	R = MeOH	R = ACN	R = MeOH	R = ACN
B + H	100	72	5	0.3
B + H + R	63	100	100	35
B + H + 2R	0.9	68	69	100
B + H + 3R	–	2	1	6
B + H + H_2O	16	0.6	14	0.1
B + H + $2H_2O$	–	–	7	–
B + H + AcOH	9	0.3	19	0.1
B + H + R + H_2O	0.6	1	47	2
B + H + 2R + H_2O	–	–	1	0.2
2B + H	97	7	28	–
2B + H + R	–	0.7	11	–
2B + H + H_2O	–	–	7	–

TABLE III

TXB RELATIVE ION ABUNDANCES

TSP mode, filament on; positive-ion detection; ion source, 250°C. Eluent, 50% BUTAC (0.1 *M*)–methanol at 1 ml/min.

$[Assignment]^+$	Ion	*m/z*	Relative abundance
X + $BuNH_3$ – H_2O	3	226	6
T + $BuNH_3$	5	230	2.5
X + $BuNH_3$	6	244	100
Y + $BuNH_3$ – H_2O	8	252	46
Y + $BuNH_3$	12	270	87
Z + $BuNH_3$	13	272	2.9
U + $BuNH_3$ – $2H_2O$	25	364	0.5
U + $BuNH_3$ – 30	27	370	2.2
U + $BuNH_3$ – H_2O	29	382	2.6
M + $BuNH_3$ – $3H_2O$	30	390	5.1
U + $BuNH_3$	33	400	0.2
M + $BuNH_3$ – $2H_2O$	34	408	1.2
M + $BuNH_3$ – H_2O	36	426	1.0
M + $BuNH_3$	38	444	1.8

TABLE IV

TXB AND DTXB METHYL ESTERS AND TXB METHOXIME (TXBMO)

TSP mode, filament on; positive-ion detection; ion source, 250°C. Eluent, 40% AMAC (0.1 *M*)–methanol at 1 ml/min.

[Assignment]$^+$	Ion No.	*m/z*			Relative abundance		
		TXB	DTXB	TXBMO	TXB	DTXB	TXBMO
X + NH_4 − H_2O	3	184	156	170	–	–	0.4
X + H	4	185	157	171	10	11	4.1
T + NH_4	5	174	X[a]	174	5.8		4.2
X + NH_4	6	202	174	188	100	100	100
V + H − CH_3OH	7	X[a]	X[a]	194	–	–	3.8
Y + NH_4 − H_2O	8	210	182	196	7.2	12	36
Y + H	9	211	183	197	6.8	7.1	–
V + NH_4 − MeOH	11	X[a]	X[a]	211	–	–	57
Y + NH_4	12	228	200	214	73	88	5.6
V + H	15	X[a]	X[a]	226		–	3.3
V + H + H_2O	16	X[a]	X[a]	244	–	–	2.2
R + H − H_2O	18	277	249	263	5.8	12	1.2
R + NH_4 − H_2O	21	294	266	280	1.4	1	–
U + H − $2H_2O$	22	305	277	291	3.6	2.7	–
R + NH_4	24	312	284	298	0.8	1	1.2
U + NH_4 − $2H_2O$	25	322	294	308	0.5	0.5	–
U + H − H_2O	26	323	295	337	3.3	5	–
U + NH_4 − 30	27	328	300	314	1.6	1.5	3.8
M + H − $3H_2O$	28	331	303	346	49	48	1.0
U + NH_4 − H_2O	29	340	312	326	5.9	7.3	–
M + NH_4 $3H_2O$	30	348	320	363	9.9	9.1	–
M + H − $2H_2O$	31	349	321	364	27	22	4.4
M + NH_4 − 32 − H_2O	32	352	324	367	–	–	1.6
U + NH_4	33	358	330	344	9.6	20	–
M + NH_4 − $2H_2O$	34	366	338	381	28	24	–
M + H − H_2O	35	367	339	382	17	26	32
M + NH_4 − H_2O	36	384	356	399	29	73	2.0
M − H	37	385	357	400	6	17	–
M + NH_4	38	402	374	417	10	25	–

[a] The corresponding *m/z* ions should not be expected.

derivatives, as in Tables III–IV. The same system is used in Tables V and VI for negative ions.

A tentative assignment of the ions detected is also shown in Table I. Assignment of the more abundant ions in the low-mass range was made assuming that these ions can be explained as proposed in Eqn. 1, M being a fragment from TXB or DTXB. In this way, the groups of ions 3, 4, 6 and 14 and 8, 9, 12 and 17 can be related to two families arising from two fragments with molecular masses of 170 (142 for DTXB) and 196 (168 for DTXB). These two fragments are called X and

TABLE V

TXB AND DTXB RELATIVE ION ABUNDANCES

TSP mode, negative-ion detection; ion source, 250°C. Eluent, 50% AMAC (0.1 *M*)–MeOH at 1 ml/min.

[Assignment]$^-$	Ion No.	*m/z*		Relative abundance			
		TXB	DTXB	Filament on		Filament off	
X − H	1	169	141	2.3	6.3	9.2	16.2
X	2	170	142	4.9	4.0	–	–
Y − H	4	195	167	3.9	12	34	35
Y	5	196	168	55	13	–	–
T + FO	6	201	X[a]	1.8	–	–	–
T + FOH	7	202	X[a]	1.4	–	–	–
X + FO	10	215	187	20	78	77	82
X + FOH	11	216	188	41.2	48	–	–
T + FO	13	X[a]	201	2.2	5.7	–	3.5
T + FOH	14	X[a]	202	2.5	4.4	–	–
Y + FO	16	241	213	28	100	99	100
Y + FOH	17	242	214	100	91	–	–
Y + AcO	18	255	227	1.7	5.6	–	7.4
Y + AcOH	20	256	228	5.2	5.1	–	–
U − H − H_2O	25	307	279	1.2	3.2	5.9	6.1
U − H_2O	26	308	280	2.2	3.8	–	–
M − H − $2H_2O$	30	333	305	1.7	3.6	3.5	6.0
M − $2H_2O$	31	334	306	1.8	3.5	–	–
U + FO − 30	33	341	313	1.4	3.5	–	2.6
M − H − H_2O	35	351	323	4.0	3.2	2.4	4.5
M − H_2O	36	352	324	3.9	2.5	–	–
M − H	42	369	341	22	29	100	52
M	43	370	342	6.2	4.8	–	–
M + FO	49	415	387	6.7	5.0	14	6.7

[a] The corresponding *m/z* ions should not be expected.

Y. Also, ions 29 and 33 in the high-mass range (quasimolecular zone) were assigned to adducts from a fragment U with a molecular mass of 326 a.m.u. (298 for DTXB). Fragment T adducts, assigned according to the data shown in Tables I, III and IV, will be discussed later, as well as ions 13 and 27.

Further confirmation of the adduct assignments in Table I can be assessed using other bases instead of ammonia in the HPLC eluent. Methylammonium buffers have been used in this way for identification purposes [7]. In comparison with the AMAC buffer, the use of N-alkylamines produces spectral patterns with $[M + BaseH]^+$ adducts shifted by $14n$ mass units, but with unchanged $[M + H]^+$ adducts. With BUTAC, the total response diminished approximatetively five-fold relative to ammonium or ethylammonium buffers (results not shown). However, the more drastic shifts obtained with this base (56 mass units) make it more

TABLE VI

TXB AND DTXB METHYL ESTERS AND TXB METHOXIME (TXBMO)

TSP mode, filament on, except for TXBMO; negative-ion detection; ion source, 250°C. Eluent: 50% AMAC (0.1 *M*)–ACN at 1 ml/min.

[Assignment]$^-$	Ion No.	*m/z*			Relative abundance		
		TXB	DTXB	TXBMO	TXB	DTXB	TXBMO
V − CH_3OH − H	3	X[a]	X[a]	192	–	–	7
Y − H	4	209	181	194	–	–	2
T + FO	6	201	X[a]	201	8	–	–
X + FO	10	229	201	215	–	–	8
V − CH_3OH + FO	15	X[a]	X[a]	238	–	–	25
Y + FO	16	255	227	240	–	–	5
V − CH_3OH + H_2O + FO	19	X[a]	X[a]	256	–	–	3
U − H − 30	23	309	281	295	–	–	27
M − H − CH_3OH − $2H_2O$	24	X[a]	X[a]	330	–	–	6
U − H − H_2O	25	321	293	307	–	–	17
M − $3H_2O$	27	330	302	345	100	99	–
M − H − CH_3OH − H_2O	28	X[a]	X[a]	348	–	–	26
U − H	29	339	311	325	–	–	2
M − H − $2H_2O$	30	347	319	362	4	–	–
M − $2H_2O$	31	348	320	363	24	37	–
M − H − CH_3OH	32	X[a]	X[a]	366	–	–	14
U + FO − 30	33	355	327	341	–	–	10
M + FO − CH_3OH − H_2O	34	X[a]	X[a]	376	–	–	3
M − H − H_2O	35	365	337	380	–	–	11
M − H_2O	36	366	338	381	4	5	–
U + FO − CH_3OH	37	X[a]	X[a]	353	–	–	9
M + FO − $3H_2O$	38	375	347	390	2	–	–
M + FOH − $3H_2O$	39	376	348	391	6	6	–
M + FO − CH_3OH − H_2O	41	X[a]	X[a]	394	–	–	10
M − H	42	383	355	398	–	2	100
M	43	384	356	399	8	4	–
M + FO − $2H_2O$	44	393	365	408	2	4	–
M + FOH − $2H_2O$	45	394	366	409	11	14	–
M + FO − CH_3OH	46	X[a]	X[a]	412	–	–	3
M + FO − H_2O	47	411	383	426	15	22	6
M + FOH − H_2O	48	412	384	427	13	24	–
M + FO	49	429	401	444	60	100	10
M + FOH	50	430	402	445	24	25	–

[a] The corresponding *m/z* ions should not be expected.

appropriate for identification purposes. The reagent ion plasmas from BUTAC and AMAC in 50% methanol and ACN are shown in Table II.

The mass spectrum of TXB in BUTAC is shown in Table III. Major ions 6 and

12 (see also Table I) are shifted by 56 mass units corresponding to the $[X + BuNH_3]^+$ (244) and $[Y + BuNH_3]^+$ (270) adducts (Bu = butyl), and the signals at 188 and 214 have disappeared. Similar considerations can be made for the base adducts from fragment U and TXB quasimolecular ions.

TSP mass spectra of TXB and DTXB methyl esters are in agreement with the data shown above. As shown in Table IV, methyl esters show more abundant ions in the quasimolecular ion zone than free acids. All the ions are shifted by 14 mass units due to the methyl group, except for ion 5 at *m/z* 174 in Table IV. Ion 5 is also observed in free TXB and DTXB at this same *m/z* (Table I) and is shifted by 56 mass units with BUTAC buffer (Table III). Accordingly, ion 5 would be an ammonia adduct from a fragment that does not contain the carboxylic lateral branch. Further, ions arising by losses of 44 mass units (CH_2CHOH) from the M adducts (fragment U, ions 25, 29 and 33) are clearly visible in the methyl ester spectra and are also present in the mass spectra of the free compounds (Tables I and III). A possible pathway for the formation of U is shown in Fig. 2 (path a) as a retrograde aldol condensation (RAC) from the open form of the hemiketal ring. In addition, the proposed structure for U can account for the formation of fragments X and T as shown in the figure (path c). X and T can also be formed directly from the intact molecule (Fig. 2, path b). In a similar way, a retro-Diels–

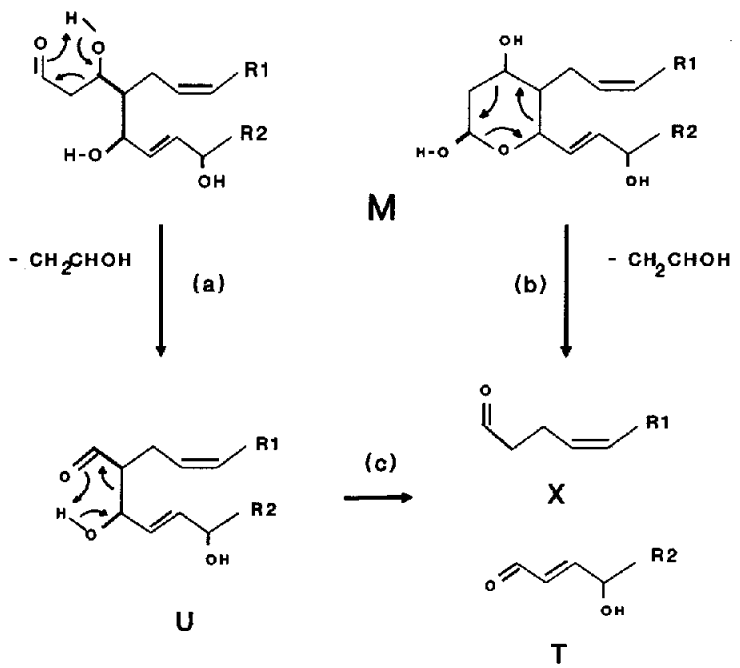

Fig. 2. Visualization of the fragmentation of TXB and DTXB to afford fragments U (path a) and X and T (paths b and c). R1 and R2 as in Fig. 1. For methyl ester derivatives R1 = $(CH_2)_3COOCH_3$ (TXB) or CH_2COOCH_3 (DTXB). An equivalent mechanism can be visualized for methoxime derivatives.

Alder mechanism (RDA) from a dehydrated form of TXB and DTXB can account for the formation of fragments Y and T (Fig. 3).

An important ion (18 in Table IV) at 277 for TXB and at 249 for DTXB is observed in the spectra of methyl esters. Ion 18 as well as ions 21 and 24 in Table IV can be explained as adducts arising from a fragment of 294 a.m.u. (fragment R). Although these ions could be expected in the mass spectra of underivatized compounds, they were not observed. However, they are present in the spectra from the methoximated derivatives, as discussed below. A possible visualization of the formation of this fragment is shown in Fig. 4.

Methoxime derivatives of TXB and DTXB show more complex TSP mass spectra (Table IV). In addition to ions arising from fragments X, Y, T, U and R, methoximes show adducts from a fragment V and losses of methanol from the methoxime group. The principal fragmentation pathways for the nitrogen-containing fragments of methoximes are shown in Fig. 5. Fragment V is the corresponding methoxime of Y (Fig. 3), and the presence of V and V-32 in the spectra supports the structure shown for Y with the carbonyl group at position C-11. As reported previously, methoxime derivatives of prostaglandins with keto groups readily hydrolyse in the interface with loss of the methoxime group [5]. In this case, methoxyamine losses from the non-fragmented structures or from V account for the presence of Y in these spectra. In addition, losses of methanol, not observed in the TSP spectra of prostaglandin derivatives, represent the more important process from the methoxime moiety of the aldehyde group on TXB and DTXB.

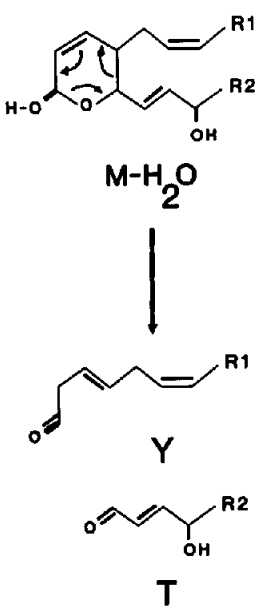

Fig. 3. Visualization of the formation of Y and T through an RDA rearrangement from a dehydrated form of TXB or DTXB. R1 and R2 as in Fig. 1.

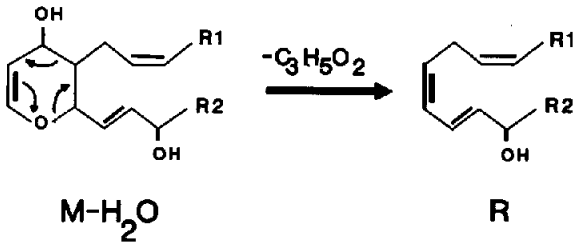

Fig. 4. Visualization of the formation of fragment R through an RDA rearrangement from a dehydrated form of TXB or DTXB. R1 and R2 as in Fig. 1.

Temperature and solvent effects

A shown in Table I, major signals of TXB and DTXB correspond to ions 6 and 12 whereas only low-abundant ions are observed in the quasimolecular ion zone. This spectral pattern is similar at all the source temperatures tested (200, 250 and 300°C). A major difference is observed in the relative abundance of ion 12 at the two temperatures listed in Table I.

The interface temperature has a more drastic effect on the spectral pattern of these compounds (results not shown). At low interface temperatures low-mass ions are dominant, but near the total vaporization temperature, ions in the quasimolecular ion zone become more abundant. Further, these ions are dehydration adducts from the parent compounds, and the $[M + H]^+$ and $[M + NH_4]^+$ ion abundances remain practically constant at all the interface temperatures.

Two possible mechanisms can account for these facts: first, dehydration processes in the interface at high temperatures compete with fragmentation

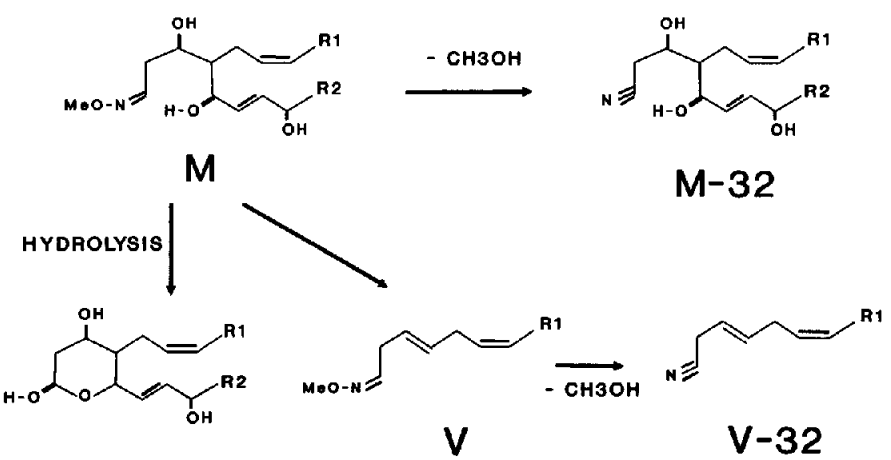

Fig. 5. Visualization of the principal fragmentation pathways for methoxime derivatives leading to nitrogen-containing fragments.

processes, which are the dominant pathways from the intact molecule. Second, if fragments are formed from thermal degradation in the interface (source temperature does not significantly affect spectral pattern), different volatilities of fragments relative to the high-mass compounds can favour their ionization at lower temperatures.

The importance of the dehydration processes in the fragmentation of these compounds is reflected in the relative abundance of adducts from fragment Y relative to those from fragment X at different interface temperatures (data not shown in Tables). At low interface temperatures, the relative abundance of ions 6 and 12 for TXB is 10/6 and becomes 3/10 at high temperatures. As shown in Figs. 2 and 3, formation of Y can be explained as a RDA reaction from a dehydrated form in C-9 and X can be formed in a similar way from the intact ring (or through U). Thus, at high interface temperatures, when dehydration would be an important process in the TSP interface, formation of fragment X is dificulted in comparison to fragment Y.

Formation of ions resulting from hydrolysis of the methoxime group and losses of methanol is also affected by interface temperature in methoxime derivatives. At low interface temperatures, major ions in the quasimolecular zone correspond to $[M + H - H_2O]^+$ and $[M - CH_3OH + NH_4 - H_2O]^+$ but at high temperatures only ions from hydrolysis in addition to abundant $[M + H - H_2O]^+$ and $[M + H - 2H_2O]^+$ are observed.

Solvent effects are also observed in the spectra of these compounds. Methanol-containing buffers afford spectra with abundant fragment ions. In contrast, ACN yields ions in the quasimolecular ion zone with abundant adducts from dehydration processes. This effect is also observed in prostaglandin mass spectra and can be related to the different capabilities of the buffers to solvate the ions and form hydrogen bridges. This is in agreement with the observed fact that dehydration processes compete with fragment formation.

Further, BUTAC buffer produces more abundant $[Y + BaseH - H_2O]^+$ and $[X + BaseH - H_2O]^+$ ion adducts than ammonium buffers, both in ACN- and methanol-containing buffers. Losses of water from the $[Y + BaseH]^+$ adduct correspond to 50% of the parent ion abundance in methanol, and become the base peak in ACN. The fact that fragments X and Y do contain not a hydroxy but an aldehyde group suggests that an imine group is formed between the base and the carbonyl moiety. In the liquid phase, butylamine is more basic than ammonia and a better nucleophile; also, alkylimines are more stable to hydrolysis than imines, which could account for the different proportions in which these ions are formed in the two buffers.

In general, discussion of ionization in TSP should take into consideration the relative acid–base characteristics of the compounds entering the interface (proton affinities in gas or liquid phase for chemical ionization or ion desorption processes, respectively). Care must be exercised when additional moieties from chemical reactions between analyte and reagent plasma can be formed. In this case, it is not

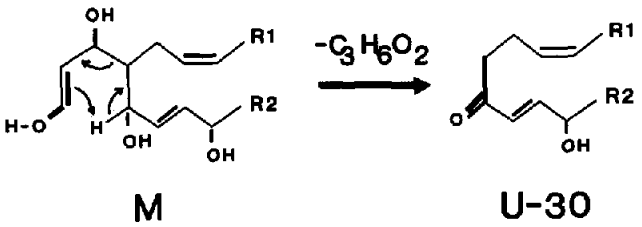

Fig. 6. Visualization of the formation of fragment U − 30. R1 and R2 as in Fig. 1.

the carbonyl group of the aldehyde that directs ionization by adduct formation with the protonated base but the more basic imine group.

Figs. 2–6 show a visualization of the more abundant fragment formation schemes. It must be noted that each adduct ion can correlate with more than one chemical structure. For example, losses of water can take place at different carbon atoms, C-9, C-11, C-12 and C-15, affording at least four possible structures for the $[M + H - H_2O]^+$ adducts with different fragmentation behaviour.

Similar fragmentation pathways in fast-atom bombardment (FAB) MS have been reported by other authors for these types of structure [9,10]. Lhoest *et al.* [8] proposed an RDA reaction for the fragmentation of a six-membered hemiketal ring, and Dallinga and Heerma [9] proposed similar mechanisms for the fragmentation of the negative and positive ions of some aldohexoses and deoxyaldohexoses in FAB-MS and FAB-MS–MS.

Whether these fragmentations take place in the gas or liquid phase, and from charged or neutral molecules, is not clear from our data. Further, TXB in the liquid phase is in equilibrium with its free aldehyde form, and similar fragmentation processes should take place throughout the open structure.

Negative-ion spectra

Negative-ion mass spectra of TXB and DTXB are shown in Table V. Spectra obtained in the filament-off mode are characterized by signals due to losses of H^+ from M and/or formate adducts with M as well as with fragments X, Y, T and U. As can be expected from the presence of the carboxyl group in X, Y and U, all these fragments show ions generated by the loss of a proton. Formate adducts are dominant over those from acetate, which account only for 1–10% of the total anion attachment. Formate adducts are the more abundant ions at low source temperatures (200–250°C) but at 300°C the loss of a proton becomes the more important mechanism.

In the filament-on mode, important signals from electron-capture processes are observed. Owing to the lack of groups with high electron affinity in the molecule the system was tested for possible detuning effects. The Hewlett-Packard acquisition software shows some unresolved features that can account for mass assignment errors. (a) Each acquisition mode (positive and negative ions in filament-on or -off mode) must be run with a different tuning programme, and it is

not possible to switch between filament on and off in the same run. This applies to other parameters, such as repeller voltage and also electron energy, which cannot be scanned either manually or automatically during the acquisition. (b) Despite the fact that ion masses are stored with a decimal number, data processing shows two different mass spectral representations. For example, for an ion at 265.65 (M − 1 for adenosine in negative-ion mode, filament off) with the high decimal point value due to a detuning effect, tabulation from a scan shows this mass value with the correct decimal point, but tabulation from an average, background substraction or normalization process affords a surprising result: mass values seem to be weighted for the decimal point and then rounded. In this way the spectrum shows not one signal at 266 or 265.7 but two signals at 265 and 266 with relative abundances of 1/2.

With this effect in mind, tuning parameters optimized for acquisition with filament off were used for acquisition with the filament on and mass axis was tested between runs using PPG and during the acquisition by monitoring known plasma ions. Despite a slightly decreased total sensitivity obtained in this way, no differences in relative ion abundances were found.

Similar spectra showing ions from odd-electron species have been obtained for prostaglandins (PGs) $F_{2\alpha}$, E_2, D_2, B_2 and 6-keto-prostaglandin $F_{1\alpha}$ as well as for unsaturated α- and γ-ketohydroxy acids derived from linoleic acid (data not shown). Although TSP mass spectra of prostanoids and TXB in the negative mode have been reported earlier [2], the electron-capture process was not described, possibly owing to experimental differences because electron capture would be very dependent on the physical and thermodynamic characteristics of the TSP plume and ion source.

Some general facts that can be outlined are as follows. (a) Source pressure and TSP plume characteristics affect electron capture, possibly by electron thermalization and or electron–molecule interaction effectiveness. Electron-capture ions are dominant at low source and interface temperatures (Fig. 7). (b) No important differences can be observed using methanol or ACN in the relative abundance of electron capture and even-electron ions. (c) Losses of water favour electron capture; M^- ions (and $[M + FOH]^-$) have low abundances or can be explained as isotopic signals from the $[M - H]^-$ ion. An exception in the prostaglandin series is PGB_2, a dehydrated form of PGE_2 with a conjugated ketone in its structure. In this way, dehydration affords conjugated systems able to stabilize the electron.

The carboxylate anion accounts for the overall ions arising from proton losses. These ions are practically absent in methyl ester spectra (Table VI), in which base peaks are due to formate adducts and electron-capture processes.

Mass spectra of methoxime derivatives are shown in Table VI. An important fragment at 295 a.m.u. ($[U - H - 30]^-$, ion 23) is observed in these spectra. U − 30 fragment adducts have also been detected in positive- and negative-ion mode with variable abundances (see Tables). Formation of the U − 30 fragment from the enolic form of the aldehyde is visualized in Fig. 6.

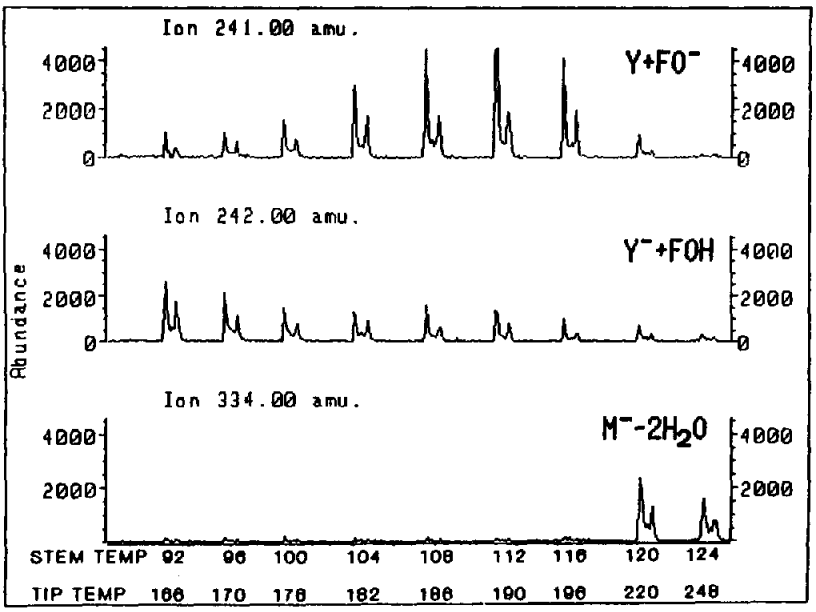

Fig. 7. Effect of the interface temperature (STEM TEMP) on the relative abundance of ions generated by processes of electron capture ($[Y + FOH]^-$), formate attachment ($[Y + FO]^-$) and from dehydration processes ($[M - 2H_2O]^-$). The chromatogram shows the total current due to each ion for consecutive TXB injections in the HPLC–MS system at different interface temperatures. The temperature at the interface exit (TIP TEMP) is also shown. The double TXB peak is due to the open–closed ring equilibrium that takes place during the chromatography. The spectra obtained from the two peaks are indistinguishable.

HPLC of TXB and DTXB

Both the non-derivatized and the methyl ester derivatives of TXB and DTXB chromatograph under the conditions specified in Experimental as a double peak (Fig. 7) characterized by the well-known "saddle" effect usually observed in the chromatography of compounds affected by the existence of different equilibrium forms in solution. This effect can usually be minimized by speeding the separation process to diminish the time available for equilibrium interchange [10]. This would be the main limitation in the HPLC analysis of TXB and even though by proper optimization of parameters such as total time of chromatography, pH and ionic strength this can often be improved, in the case of TSP it is not possible owing to the restrictive conditions of the eluent composition. In contrast, methoxime derivatives show only one peak because, since the aldehyde group is blocked by the reagent, only one of the forms dominates the equilibrium.

CONCLUSIONS

TXB shows characteristic and different TSP behaviour relative to the other components of the arachidonic acid cascade (prostaglandins and linear chain

hydroxy acids). Some of its most important fragmentation processes can be correlated with those observed for some monosaccharides in FAB-MS. Despite this, complete elucidation of adduct structures and fragmentation mechanisms must be obtained with labelled compounds and MS–MS techniques.

The chromatographic and MS characteristics of TXB (due to the aldehyde–hemiketal equilibrium and fragmentation processes, respectively) are serious drawbacks in developing TSP analytical methods for this molecule. Data presented here suggest that focusing on fragments at masses between 200 and 250 a.m.u. can be a successful alternative to detection in the quasimolecular ion zone.

ACKNOWLEDGEMENTS

The authors thank Dr. D. Barceló and Dr. A. Messeguer for fruitful discussions, and R. Alonso for technical assistance. This work was supported by Grant 89/0386 from FIS (Spain).

REFERENCES

1 R. Richmond, S. R. Clarke, D. Watson, C. G. Chappel, C. T. Dollery and G. W. Taylor, *Biochim. Biophys. Acta*, 881 (1986) 159.
2 R. D. Voyksner and E. D. Bush, *Biomed. Environ. Mass Spectrom.*, 14 (1987) 213.
3 J. A. Yergey, H.-Y. Kim and N. Salem, *Anal. Chem.*, 58 (1986) 1344.
4 J. Abián and E. Gelpi, *J. Chromatography.*, 394 (1987) 147.
5 J. Abián, J. O. Bulbena and E. Gelpí, *Biomed. Envrion. Mass Spectrom.*, 16 (1988) 215.
6 H. Maeder, *Rapid Commun. Mass Spectrom.*, 4 (1990) 52.
7 H. Maeder, *Rapid Commun. Mass Spectrom.*, 3 (1989) 183.
8 G. Lhoest, P. Wallemacq, P. Dumont and G. Van Binst, *Spectrosc. Int. J.*, 6 (1988) 269.
9 J. W. Dallinga and W. Heerma, *Biomed. Environ. Mass Spectrom.*, 18 (1989) 363.
10 R. Freixa, J. Casas, J. Roselló and E. Gelpí, *J. High. Resolut. Chromatogr. Chromatogr. Commun.*, 7 (1984) 156.